

# 1 Hilbert Statistics of Vorticity Scaling in Two-Dimensional Turbulence

2 H.S. Tan (谭唤书),<sup>1</sup> Y.X. Huang (黄永祥),<sup>1, a)</sup> and Jianping Meng (孟剑平)<sup>2</sup>

3 <sup>1</sup>*Shanghai Institute of Applied Mathematics and Mechanics,*  
 4 *Shanghai Key Laboratory of Mechanics in Energy Engineering, Shanghai University,*  
 5 *Shanghai 200072, People's Republic of China*

6 <sup>2</sup>*James Weir Fluids Lab, Department of Mechanical and Aerospace Engineering,*  
 7 *University of Strathclyde, Glasgow G1 1XJ*

8 (Dated: 7 June 2021)

9 In this paper, the scaling property of the inverse energy cascade and forward en-  
 10 strophy cascade of the vorticity field  $\omega(x, y)$  in two-dimensional (2D) turbulence  
 11 is analyzed. This is accomplished by applying a Hilbert-based technique, namely  
 12 Hilbert-Huang Transform, to a vorticity field obtained from a  $8192^2$  grid-points di-  
 13 rect numerical simulation of the 2D turbulence with a forcing scale  $k_f = 100$  and  
 14 an Ekman friction. The measured joint probability density function  $p(C, k)$  of mode  
 15  $C_i(x)$  of the vorticity  $\omega$  and instantaneous wavenumber  $k(x)$  is separated by the forc-  
 16 ing scale  $k_f$  into two parts, which corresponding to the inverse energy cascade and  
 17 the forward enstrophy cascade. It is found that all conditional pdf  $p(C|k)$  at given  
 18 wavenumber  $k$  has an exponential tail. In the inverse energy cascade, the shape of  
 19  $p(C|k)$  does collapse with each other, indicating a nonintermittent cascade. The mea-  
 20 sured scaling exponent  $\zeta_\omega^I(q)$  is linear with the statistical order  $q$ , i.e.,  $\zeta_\omega^I(q) = -q/3$ ,  
 21 confirming the nonintermittent cascade process. In the forward enstrophy cascade,  
 22 the core part of  $p(C|k)$  is changing with wavenumber  $k$ , indicating an intermittent  
 23 forward cascade. The measured scaling exponent  $\zeta_\omega^F(q)$  is nonlinear with  $q$  and can  
 24 be described very well by a log-Poisson fitting:  $\zeta_\omega^F(q) = \frac{1}{3}q + 0.45(1 - 0.43^q)$ . How-  
 25 ever, the extracted vorticity scaling exponents  $\zeta_\omega(q)$  for both inverse energy cascade  
 26 and forward enstrophy cascade are not consistent with Kraichnan's theory predic-  
 27 tion. New theory for the vorticity field in 2D turbulence is required to interpret the  
 28 observed scaling behavior.

29 PACS numbers: 47.27.Gs, 47.57.Bc, 47.53.+n

---

<sup>a)</sup>Electronic mail: yongxianghuang@gmail.com

## 30 I. INTRODUCTION

31 Two-dimensional (2D) turbulence is an ideal model for several turbulent phenomena,  
 32 such as the first approximation to the large-scale motion in atmosphere and oceans.<sup>1-5</sup> The  
 33 2D turbulence and relative problems have attracted a lot of attentions in recent years.<sup>6-18</sup>  
 34 Several review papers have been devoted to this topic in a detail, for example, papers by  
 35 Tabeling<sup>2</sup>, Kellay and Goldberg<sup>3</sup>, Boffetta and Ecke<sup>4</sup>, Bouchet and Venaille<sup>5</sup>, Van Heijst  
 36 and Clercx<sup>19</sup>, to quote a few. The 2D Ekman-Navier-Stokes equation is written in term of  
 37 a single scalar vorticity field  $\omega = \nabla \times \mathbf{u}$  as, i.e.,

$$\partial_t \omega + \mathbf{u} \bullet \nabla \omega = \nu \nabla^2 \omega - \alpha \omega + f_\omega \quad (1)$$

38 in which  $\nu$  is the fluid viscosity,  $\alpha$  is the Ekman friction and  $f_\omega$  is an external source of energy  
 39 inputing into the whole system.<sup>20,21</sup> Specifically for the small scale motions, it is believed  
 40 that there exists a dual-cascade, i.e., a forward enstrophy cascade, in which the enstrophy  
 41 (square of vorticity  $\omega^2$ ) is transfered from large to small scales, and an inverse energy cascade,  
 42 in which the energy is transfered from small to large scales.<sup>22</sup> A two-power-law behavior is  
 43 thus expected to describe this dual cascade, i.e.,

$$E_u(k) = \begin{cases} C (\epsilon_\alpha)^{2/3} k^{-5/3}, & \text{when } k_\alpha \ll k \ll k_f \text{ for inverse energy cascade} \\ C' (\eta_\nu)^{2/3} k^{-3}, & \text{when } k_f \ll k \ll k_\nu \text{ for forward enstrophy cascade} \end{cases} \quad (2)$$

44 in which  $E_u(k)$  is Fourier power spectrum of the velocity,  $\epsilon_\alpha$  is the energy dissipation by  
 45 the Ekman friction,  $\eta_\nu$  is the enstrophy dissipation by the viscosity,  $k_f$  is the forcing scale,  
 46 in which the energy and enstrophy is injected into the system, and  $k_\alpha$  is the characteristic  
 47 friction scale,  $k_\nu$  is the viscosity scale. One can relate the vorticity statistics with the velocity  
 48 one by using  $E_\omega(k) \sim k^2 E_u(k)$ . Therefore, a dual power-law behavior is also expected for  
 49 the vorticity field, i.e.,

$$E_\omega(k) \sim k^2 E_u(k) \sim \begin{cases} k^{1/3}, & \text{when } k_\alpha \ll k \ll k_f \text{ for inverse energy cascade} \\ k^{-1}, & \text{when } k_f \ll k \ll k_\nu \text{ for forward enstrophy cascade} \end{cases} \quad (3)$$

50 It is found experimentally that the pdf of the velocity increment  $\Delta_\ell u$  is Gaussian when the  
 51 separation scale  $\ell$  lies in the inverse energy cascade, indicating nonintermittent behavior on  
 52 these scales.<sup>2-5,19</sup> Note that the classical structure-function (SF) analysis fails when the slope  
 53  $\beta$  of the Fourier power spectrum is out of the range  $1 < \beta < 3$ , in which  $E(k) \sim k^{-\beta}$ .<sup>23,24</sup>

54 This unfortunately is the case of the forward enstrophy cascade in the 2D turbulence.<sup>4,25</sup>  
 55 Therefore, the intermittent property of the forward enstrophy cascade can not be verified di-  
 56 rectly by using the SF analysis.<sup>20,25</sup> Kellay, Wu, and Goldberg<sup>26</sup> performed an experimental  
 57 measurement of the velocity and vorticity field of the 2D soap turbulence. They found that  
 58 the Fourier power spectrum of the velocity shows a  $-3$  power-law for the forward enstro-  
 59 phy cascade, which agrees very well with the theory. However, the corresponding Fourier  
 60 power spectrum of the vorticity field for the forward enstrophy cascade demonstrates a  $-2$   
 61 power-law, which is contradicted with the theoretical prediction, see Eq. (3). For the veloc-  
 62 ity measurement, Paret, Jullien, and Tabeling<sup>27</sup> also observed  $-3$  scaling for the forward  
 63 enstrophy cascade. Moreover, the measured pdf of vorticity increment  $\Delta_\ell \omega$  is not significant  
 64 deviation from the Gaussian distribution, i.e., a nonintermittent forward enstrophy cascade.  
 65 On the contrary, Nam *et al.*<sup>28</sup> found that if an Ekman friction coefficient  $\alpha$  is presented, the  
 66 forward enstrophy cascade is then intermittent.<sup>29</sup> Boffetta *et al.*<sup>20</sup> argued that if a passive  
 67 scalar  $\theta$  is governed by the same equation as the vorticity field and if it is also advected by  
 68 the same velocity field, it then can be taken as a surrogate of the vorticity  $\omega$  for the small  
 69 scale statistics. They found that the passive scalar  $\theta$  is indeed intermittent. Moreover, they  
 70 found that the fitting scaling exponent for the forward enstrophy cascade is dependent on  
 71 the Enkman viscosity  $\alpha$ . Later, Tsang *et al.*<sup>30</sup> studied the intermittency of the forward  
 72 enstrophy cascade regime with a linear drag. The relative scaling exponent  $(\zeta(2q)/\zeta(2))$   
 73 provided by the vorticity SF confirms that the forward enstrophy cascade is intermittent for  
 74 the considered statistical order  $0 \leq q \leq 2$ . Note that the classical SF approach is employed  
 75 in their studies. Biferale *et al.*<sup>25</sup> proposed an inverse velocity statistics and applied in 2D  
 76 turbulence. They found that the velocity fluctuation can not be simply described by one  
 77 single exponent, indicating an intermittent forward cascade. Boffetta<sup>21</sup> reported that the  
 78 fitting scaling exponent of the Fourier power spectrum for the forward cascade might also  
 79 depend on the viscosity  $\nu$ . Recently, Falkovich and Lebedev<sup>31</sup> derived analytically the prob-  
 80 ability density function (pdf) for strong vorticity fluctuations (resp. the tail of the pdf) in  
 81 the forward enstrophy cascade. They found that the over  $R$  coarse-grained vorticity  $\bar{\omega}(R)$   
 82 has a universal asymptotic exponential tail and is thus self-similar without intermittency  
 83 (resp. scaling exponent is linear with  $q$ ) at least for high-order statistics. Generally speaking,  
 84 Kraichnan's theory of 2D turbulence is partially confirmed by the experiments and numer-  
 85 ical simulation for the velocity field.<sup>32</sup> However, as mentioned above, the statistics of the

86 vorticity field seems to disagree with the theoretical prediction.

87 In this paper, we apply a Hilbert-based technique to the vorticity  $\omega(x, y)$  field obtained  
88 from a high resolution direct numerical simulation (DNS). A dual-cascade behavior is ob-  
89 served respectively with a nearly one decade inverse energy cascade and forward enstrophy  
90 cascade. For the inverse energy cascade, the measured vorticity pdf does collapse with each  
91 other, implying a nonintermittent cascade process as expected.<sup>4,5,31</sup> The corresponding mea-  
92 sured scaling exponent  $\zeta_{\omega}^I(q)$  is linear with  $q$ , i.e.,  $\zeta_{\omega}^I = q/3$ . For the forward enstrophy  
93 cascade, the measured vorticity pdf possesses an exponential tail, which is consistent with  
94 the findings in Ref.<sup>31</sup>. However, they can not collapse with each other, indicating an in-  
95 termittent forward enstrophy cascade. The measured scaling exponent  $\zeta_{\omega}^F(q)$  is nonlinear  
96 with a small  $q$  and asymptotic to a linear relation for large  $q$ . A log-Poisson-like formula  
97 is proposed to describe the measured scaling exponent, i.e.,  $\zeta_{\omega}^F = q/3 + 0.45(1 - 0.43^q)$  for  
98 the forward enstrophy cascade. Note that for the vorticity field, the measured scaling expo-  
99 nents disagree with the theoretical prediction by Kraichnan<sup>22</sup> even one takes the logarithmic  
100 correction into account. New theory about the vorticity field is required to interpret our  
101 findings in this work.

## 102 II. HILBERT-HUANG TRANSFORM

### 103 A. Empirical Mode Decomposition

104 The method we used in this work is the so-called arbitrary-order Hilbert spectral  
105 analysis.<sup>33,34</sup> It is an extended version of the Hilbert-Huang Transform (HHT).<sup>35,36</sup> The  
106 Hilbert method contains two steps. In the first step, a data-driven algorithm, namely Em-  
107 pirical Mode Decomposition (EMD), is designed to decompose a given signal, e.g.,  $\omega(x)$ ,  
108 into a sum of Intrinsic Mode Functions (IMFs)  $C_i(x)$  without *a priori* basis.<sup>35,37</sup> The IMF  
109 is an approximation of the mono-component signal, which has to satisfy the following two  
110 conditions: (i) the difference between the number of local extrema and the number of zero-  
111 crossings must be zero or one; (ii) the running mean value of the envelope defined by the  
112 local maxima and the envelope defined by the local minima is zero.<sup>35,36,38</sup> The extracted  
113 IMF mode possesses a well-behave Hilbert spectrum with a physical meaningful instanta-  
114 neous frequency in time domain (resp. wavenumber in space domain).<sup>35,36</sup> Figure 1 shows

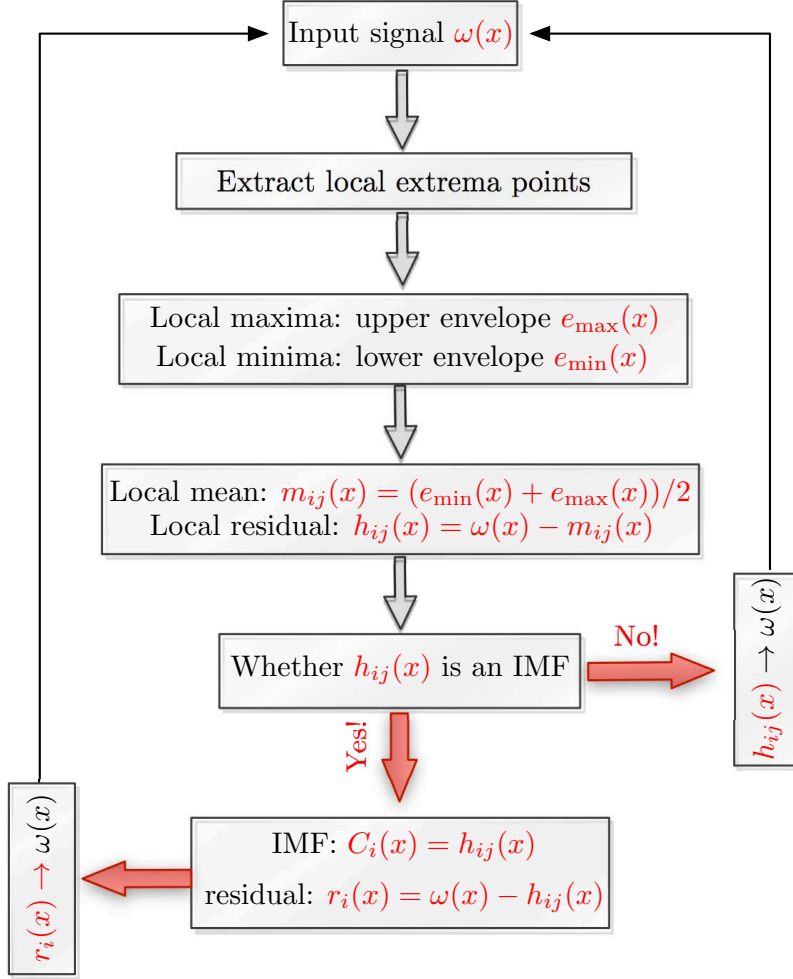


FIG. 1. (Color online) A flowchart of the Empirical Mode Decomposition algorithm to show how to decompose a given vortex field  $\omega(x, y)$  at certain  $y$  into a sum of Intrinsic Mode Functions  $C_i(x)$ .

115 a flowchart of the EMD algorithm to demonstrate how to decompose a given vortex signal  
116  $\omega(x)$  into a sum of IMF modes, i.e.,

$$\omega(x) = \sum_{i=1}^N C_i(x) + r_N(x) \quad (4)$$

117 in which  $r_N(x)$  is residual. There exist several criteria to stop the sifting process and  
118 to determine whether an IMF mode is retrieved.<sup>35,36,38</sup> For example, Huang *et al.*<sup>35</sup> has  
119 proposed a Cauchy like criteria computed from two consecutive sifting, i.e.,

$$SD = \frac{\int [h_{i(j-1)}(x) - h_{ij}(x)]^2 dx}{\int [h_{i(j-1)}(x)]^2 dx} \quad (5)$$

120 in which  $h_{ij}(x)$  is the residual by removing the running mean  $m_{ij}(x)$  constructed by using  
 121 upper  $e_{\max}(x)$  and lower envelopes  $e_{\min}(x)$ . Here  $e_{\max}(x)$  (resp.  $e_{\min}(x)$ ) is the upper en-  
 122 velope constructed by using the local maxima points (resp. minima points). A typical  
 123 value can be set between 0.2 and 0.3 to provide a physical meaningful IMF mode. Another  
 124 widely used stopping criteria is proposed by Rilling, Flandrin, and Gonçalvès<sup>38</sup>. They in-  
 125 troduced an amplitude function  $a(x) = (e_{\max}(x) - e_{\min}(x))/2$  and an evaluation function  
 126  $\sigma(x) = m_{ij}(x)/a(x)$ , respectively. The sifting procedure is iterated until  $\sigma(x) < \theta_1$  for some  
 127 prescribed fraction  $(1 - \alpha)$  of the total data, while  $\sigma(x) < \theta_2$  for the rest fraction. Typical  
 128 values are  $\alpha \simeq 0.05$ ,  $\theta_1 \simeq 0.05$  and  $\theta_2 \simeq 10\theta_1$ .<sup>38</sup> A maximum iteration number, i.e., 100,  
 129 could also be used to stop the sifting. In our practice, any one of the above three criteria is  
 130 satisfied, then one IMF mode is retrieved.

## 131 B. Hilbert Spectral Analysis

132 After retrieving the IMF modes, the Hilbert spectral analysis is applied to each mode to  
 133 obtain the time-frequency information.<sup>35,36,39</sup> The Hilbert transform is defined as, i.e.,

$$\overline{C}_i(x) = \frac{1}{\pi} P \int \frac{C_i(x')}{x - x'} dx' \quad (6)$$

134 in which  $P$  means the Cauchy principle value.<sup>40,41</sup> A so-called analytical signal is then written  
 135 as, i.e.,

$$C_i^A(x) = C_i(x) + j\overline{C}_i(x) \quad (7)$$

136 in which  $j = \sqrt{-1}$ . An instantaneous wavenumber is then defined as, i.e.,

$$k_i(x) = \frac{1}{2\pi} \frac{d}{dx} \arctan \left( \frac{\overline{C}_i(x)}{C_i(x)} \right) \quad (8)$$

137 Note that Eq. (6) is a singularity transform. The differential operation is also used to define  
 138 the instantaneous wavenumber, see Eq. (8). Therefore, the Hilbert method possesses a very  
 139 local ability in the wavenumber domain. The final representation of the original data  $\omega(x)$   
 140 can be written as, i.e.,

$$\omega(x) = \sum_{i=1}^N \mathcal{A}_i(x) \exp \left( \int_{-\infty}^x j k_i(x') dx' \right) \quad (9)$$

141 in which  $\mathcal{A}_i(x) = \sqrt{\overline{C}_i(x)^2 + C_i(x)^2}$  is the modulus of  $C_i^A(x)$ .<sup>34,35</sup> Comparison with the  
 142 Fourier analysis, the above representation can be considered as a local Fourier expansion,

143 in which the amplitude  $\mathcal{A}$  and wavenumber  $k$  can be varied with  $x$ , namely amplitude- and  
 144 frequency-modulation.<sup>35</sup>

### 145 C. Arbitrary Order Hilbert Spectral Analysis

146 After obtaining the IMF modes  $C_i(x)$  and the corresponding instantaneous wavenumber  
 147  $k_i(x)$ , one can construct a set of pair  $[C_i(x), k_i(x)]$ . A  $k$ -conditional  $q$ th-order statistical  
 148 moment is then defined as, i.e.,

$$\mathcal{L}_q(k) = \left\langle \sum_{i=1}^N [C_i(x)|_{k_i(x)=k}]^q \right\rangle_x \quad (10)$$

149 in which  $\langle \dots \rangle$  is ensemble average over all  $i$  and  $x$ .<sup>34,42</sup>  $\mathcal{L}_q(k)$  could be defined by another  
 150 equivalent way as described below. One can extract a joint probability density function (pdf)  
 151 i.e.,  $p(C, k)$ , from the IMF mode  $C_i(x)$  and the corresponding wavenumber  $k_i(x)$ . Taking a  
 152 marginal integration, Eq. (10) is then rewritten as, i.e.,

$$\mathcal{L}_q(k) = \frac{\int p(C, k) |C|^q dC}{\int p(C, k) dC} \quad (11)$$

153 For a scaling process, one expects a power-law behavior, i.e.,

$$\mathcal{L}_q(k) \sim k^{-\zeta(q)} \quad (12)$$

154 in which  $\zeta(q)$  is comparable with the scaling exponents provided by the classical structure  
 155 function.<sup>34</sup>

156 The Hilbert-based methodology has been verified by using a synthesized fractional Brow-  
 157 nian motion data for mono-fractal process and a synthesized multifractal random walk with  
 158 a lognormal statistics for multifractal process.<sup>34</sup> It also has been applied successfully to  
 159 turbulent velocity,<sup>33</sup> passive scalar,<sup>24</sup> Lagrangian turbulence,<sup>42</sup> etc., to characterize the in-  
 160 termittent nature of those processes. Our experience is that the SF analysis works when  
 161  $1 < \beta < 3$  without energetic structures.<sup>24</sup> Here  $\beta$  is the scaling exponent of Fourier power  
 162 spectrum, i.e.,  $E(k) \sim k^{-\beta}$ . If  $\beta$  is out of this range, then the Hilbert methodology should  
 163 be applied to extract scaling exponents for high-order  $q$ . Moreover, due to the influence  
 164 of energetic structures, the SFs may fail even when  $\beta = 2$ . This has been found to be  
 165 the case of the three-dimensional Lagrangian turbulence.<sup>42</sup> We will show below that this is  
 166 also the case of 2D turbulence, see more discussion in Sec. III B. For more detail about the  
 167 methodology we refer the reader to the Refs. 33–35, 39, and 42.

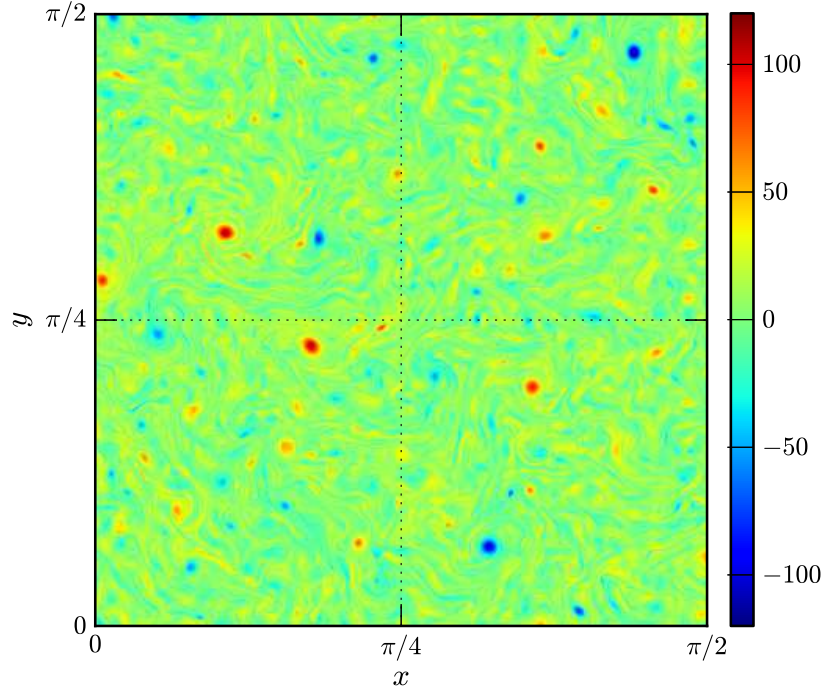


FIG. 2. (Color online) A snapshot of the vorticity field  $\omega(x, y)$  of the two-dimensional turbulence on the range  $0 \leq x, y \leq \pi/2$  from a high resolution direct numerical simulation with  $8192^2$  grid points. High intensity vorticity events are discrete distributed in space with a typical wavenumber  $k \simeq k_f = 100$  (resp. around 80 grid points).

### 169 **A. Direct Numerical Simulation of 2D Turbulence**

170 The DNS data we used in this study is provided by Professor G. Boffetta. We recall briefly  
 171 several key parameters of this simulation. Numerical integration of Eq. (1) is performed by  
 172 a pseudo-spectral, fully dealiased on a doubly periodic square domain of size  $L = 2\pi$  at  
 173 resolution  $N^2 = 8192^2$  grid points.<sup>21</sup> The main parameters are respectively  $\nu = 2 \times 10^{-6}$ ,  
 174  $\alpha = 0.025$  and  $k_f = 100$ , in which the energy is inputted into the system. The velocity  
 175 field  $\mathbf{u} = \nabla \times \Phi$  is then obtained by solving a Poisson problem  $\nabla^2 \Phi = -\omega$ , in which  $\Phi$   
 176 is a stream function. Totally, we have five snapshots with  $8192^2 \times 5 = 3.36 \times 10^8$  data  
 177 points. In the following, the analysis is done along the  $x$ -direction. This provides  $8192 \times 5 =$   
 178 40960 realizations for each statistics. The ensemble average is then averaged from all these



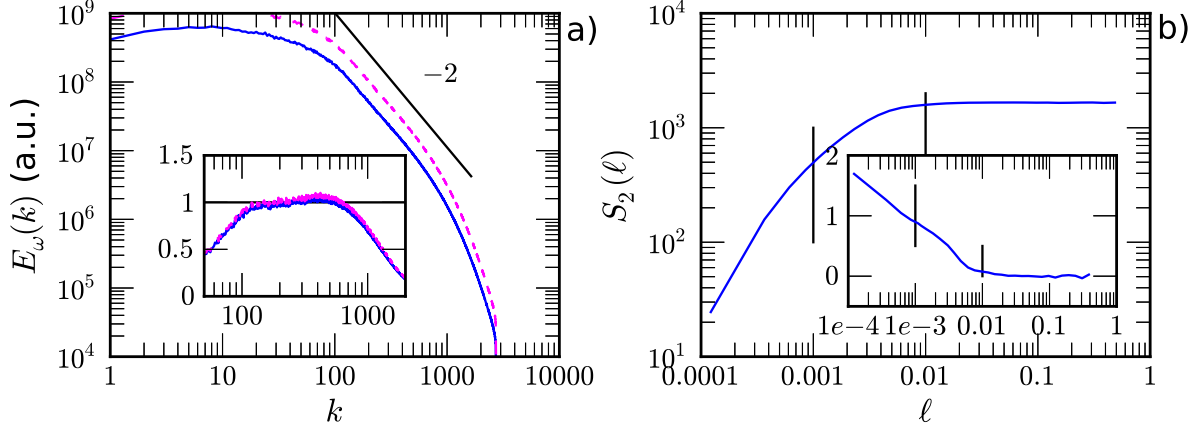


FIG. 3. (Color online) a) Measured Fourier power spectrum  $E_\omega(k)$  for vorticity field  $\omega(x, y)$ , in which a logarithmic correction  $E_\omega(k) \ln(k/k_{\min})^{-1/3}$  is shown as a dashed line. For display clarity, the measured  $E_\omega(k) \ln(k/k_{\min})^{-1/3}$  has been vertical shifted by multiplying a factor 5. A nearly one decade power-law behavior is found on the wavenumber range  $100 \leq k \leq 1000$ , corresponding to  $0.001 \leq \ell \leq 0.01$  with a scaling exponent  $\beta = 1.96 \pm 0.02$  for  $E_\omega(k)$  and  $\beta = 2.02 \pm 0.02$  for  $E_\omega(k) \ln(k/k_{\min})^{-1/3}$ , respectively. The inset shows the compensated spectrum with fitted scaling exponents. This scaling range corresponds to the forward enstrophy cascade. b) Measured second-order structure-function  $S_\omega(2, \ell)$ . No power-law behavior is observed as expected on the range  $0.001 \leq \ell \leq 0.01$ . The inset shows the local slope  $\zeta_\omega(2, \ell) = d \log_{10} S_\omega(2, \ell) / d \log_{10} \ell$  to confirming the lacking of the power-law behavior.

179 realizations. Figure 2 shows a portion of one snapshot of the vorticity field. Note that  
 180 high intensity events are discrete distributed in physical space with a typical wavenumber  
 181  $k \simeq k_f = 100$  (resp.  $\sim 80$  grid points). More detail of this database can be found in Ref. 21.

## 182 B. Fourier Power Spectrum and Second-Order Structure-Function

183 Figure 3 a) shows the measured Fourier power spectrum  $E_\omega(k)$  (solid line) of the vorticity  
 184 field, in which the logarithmic correction  $E_\omega(k) \ln(k/k_{\min})^{-1/3}$  is shown as a dashed line.  
 185 A power-law behavior for the forward enstrophy cascade is observed on the range  $100 \leq$   
 186  $k \leq 1000$ , i.e.,  $E_\omega(k) \sim k^{-\beta}$ , with a scaling exponent  $\beta = 1.96 \pm 0.02$ . The measured  $\beta$  is  
 187 consisted with the one reported by Kellay, Wu, and Goldberg<sup>26</sup>. The observed scaling range  
 188 corresponds to a spatial scale range  $0.001 \leq \ell \leq 0.01$ . The logarithmic correction provides a

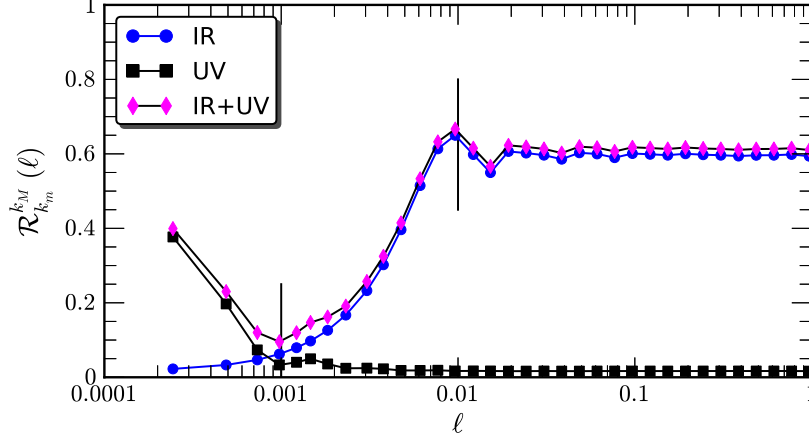


FIG. 4. (Color online) Measured relative contribution function  $\mathcal{R}_{k_m}^{k_M}(\ell)$  from different Fourier modes. Low wave number part (IR)  $[0, 100]$  ( $\circ$ ), high wavenumber part (UV)  $[1000, +\infty]$  ( $\square$ ). The expected power-law range is illustrated by a vertical solid line. Note that the expected power-law behavior is strong influenced by the low wavenumber part, known as IR effect.

189 scaling exponent  $\beta = 2.02 \pm 0.02$  on the same scaling range, showing a weak correction of the  
 190 power-law behavior.<sup>43</sup> The inset shows the corresponding compensated curves to emphasize  
 191 the observed power-law behavior. We therefore expect a power-law behavior on the range  
 192  $0.001 \leq \ell \leq 0.01$  for the second-order SFs, i.e.,

$$S_\omega(2, \ell) = \langle |\Delta_\ell \omega|^2 \rangle \sim \ell^{\beta-1} \quad (13)$$

193 in which  $\Delta_\ell \omega = \omega(x + \ell) - \omega(x)$  is vorticity increment, and  $\beta$  is the scaling exponent  
 194 from  $E_\omega(k) \sim k^{-\beta}$ . Figure 3 b) shows the measured second-order SF, in which the forward  
 195 enstrophy cascade is illustrated by a vertical solid line. Visually, no power-law behavior is  
 196 observed for the measured  $S_\omega(2, \ell)$  for the forward enstrophy cascade. To emphasize this  
 197 point, the local slope, i.e.,  $\zeta_\omega(2, \ell) = d \log_{10} S_\omega(2, \ell) / d \log_{10} \ell$ , is shown in the inset. There  
 198 is no plateau observed on the range of the forward enstrophy cascade, showing the failure  
 199 of the SFs to capture the scale invariance of the two-dimensional vorticity field.

200 To understand more about the second-order SFs  $S_\omega(2, \ell)$ , one can relate it with the  
 201 Fourier power spectrum by using Wiener-Khinchin theorem,<sup>23,24</sup> i.e.,

$$S_\omega(2, \ell) = \int_0^{+\infty} E_\omega(k) (1 - \cos(2\pi k \ell)) dk \quad (14)$$

202 in which  $E_\omega(k)$  is the corresponding Fourier power spectrum. Note that an integral constant  
 203 is neglected since it does not change the conclusion in this paper. The above equation implies

204 that the SFs contains contribution from almost all Fourier modes  $k$ . The expected power-law  
 205 behavior might be influenced by both large-scale (resp. low wavenumber, known as infrared  
 206 effect, IR) and small-scale (resp. high wavenumber, known as ultraviolet effect, UV) motions.  
 207 A partial cumulative function is therefore introduced to characterize a relative contribution  
 208 from Fourier modes band  $[k_m, k_M]$ , i.e.,

$$\mathcal{R}_{k_m}^{k_M}(\ell) = \frac{\int_{k_m}^{k_M} E_\omega(k')(1 - \cos(2\pi k'\ell)) dk'}{\int_0^{+\infty} E_\omega(k)(1 - \cos(2\pi k\ell)) dk} \quad (15)$$

209 We are particular concerned by the Fourier modes below the forcing scale, i.e.,  $[0, 100]$  (resp.  
 210 IR) and by the modes above the power-law range, i.e.,  $[1000, +\infty]$  (resp. UV). Figure 4  
 211 shows the measured  $\mathcal{R}_m^M(\ell)$  for IR ( $\circ$ ) and UV ( $\square$ ). It indicates that the SFs is strongly  
 212 influenced by the large-scale motions (resp. IR) as high as up to 65%. The expected power-  
 213 law behavior is then destroyed.<sup>24,44</sup>

214 We provide some comments on the above analysis here. The Wiener-Khinchin theorem  
 215 is only exactly valid for the linear and stationary processes. Turbulent signals in 3D or  
 216 2D are typical nonlinear and nonstationary ones. Therefore, the above argument holds  
 217 approximately here. However, this does not change the conclusion of this paper. Another  
 218 comment is for the observed high intensity vorticity event, see Fig. 2. For the high-order  
 219 SFs, they might be also influenced by those events since they usually manifest themselves at  
 220 the pdf tail of vorticity increments. This has been observed for the Lagrangian turbulence,  
 221 in which the high intensity event is known as ‘vortex trapping’ process.<sup>42,45</sup>

## 222 C. Generalization Scaling for High-Order Statistics

223 Assuming that we have SFs scaling for both the inverse and forward cascades. The  
 224 corresponding SFs and their scaling exponents without intermittent corrections are

$$S_u(q, \ell) \sim \begin{cases} \ell^{q/3}, & \text{for inverse energy cascade} \\ \ell^q, & \text{for forward enstrophy cascade} \end{cases} \quad (16a)$$

225 for the velocity field,<sup>7</sup> and

$$S_\omega(q, \ell) \sim \ell^{-q} S_u(q, \ell) \sim \begin{cases} \ell^{-2q/3}, & \text{for inverse energy cascade} \\ \ell^0, & \text{for forward enstrophy cascade} \end{cases} \quad (16b)$$

226 for the vorticity field. It implies that the forward enstrophy cascade represented by the  
 227 vorticity field is independent on the separation scale  $\ell$ . In the frame of Hilbert, we expect  
 228 the following scaling behavior for the vorticity field, i.e.,

$$\mathcal{L}_\omega(q, k) \sim \begin{cases} k^{2q/3}, & \text{for inverse energy cascade} \\ k^0, & \text{for forward enstrophy cascade} \end{cases} \quad (16c)$$

229 We will then test above relation by using the Hilbert method as we described above.

## 230 IV. HILBERT RESULTS AND DISCUSSION

### 231 A. Hilbert Statistics

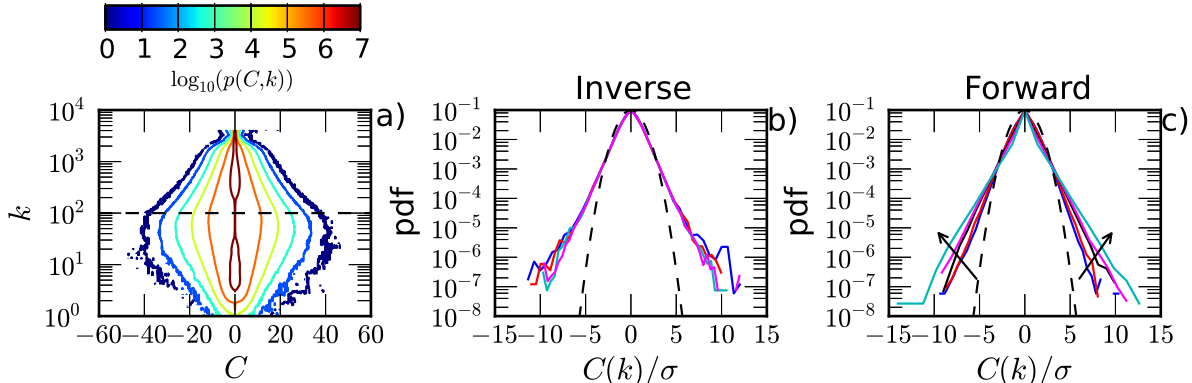


FIG. 5. (Color online) a) Contour plot of measured conditional histogram  $p(C, k)$  (resp. joint probability density function (pdf)), in which the force scale is illustrated by a dashed line. b) Measured pdf  $p(C)$  on the range  $3 < k < 20$  (resp.  $k = 4, 6, 16$  and  $20$ ) for the inverse energy cascade. c) Measured pdf  $p(C)$  on the range  $200 < k < 2000$  (resp.  $k = 250, 400, 800, 1000$  and  $1600$ ) for the forward enstrophy cascade. For comparison, the normal distribution is illustrated by a dashed line.

232 The Hilbert method is applied to the vorticity field  $\omega(x, y)$  along  $x$ -direction. The con-  
 233 ditioned/joint histogram  $p(C, k)$  (resp. probability density function if it is renormalized  
 234 properly) is extracted from all five snapshots. Figure 5a) shows the contour plot of the  
 235 measured  $p(C, k)$ , in which the forcing scale  $k_f = 100$  is illustrated by a horizontal dashed  
 236 line. For display clarity, we take the logarithm of the measured  $p(C, k)$ . It is interesting to  
 237 note that the joint pdf is roughly separated by the forcing wavenumber  $k_f = 100$  into two

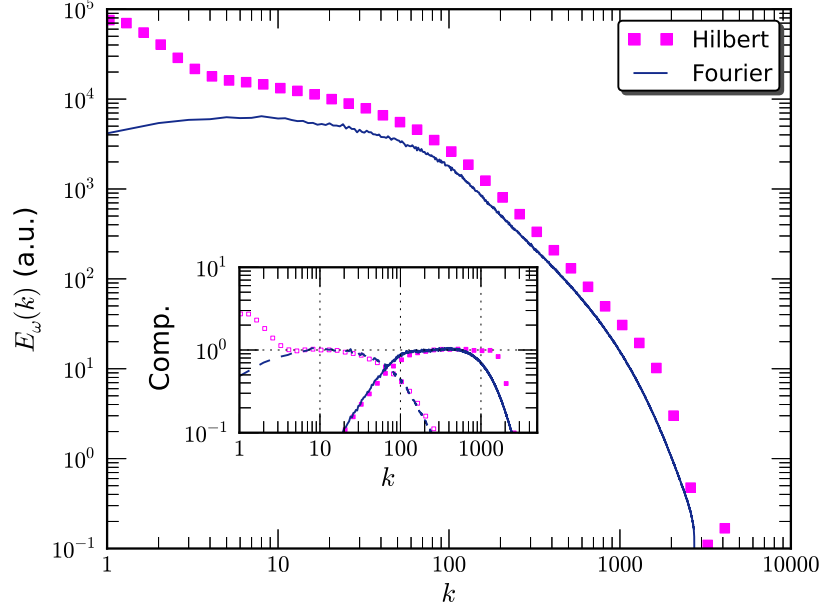


FIG. 6. (Color online) Comparison of the measured Hilbert energy spectrum  $\mathcal{L}_2(k)/k$  ( $\square$ ) and the Fourier energy spectrum  $E_\omega(k)$  (solid line). For display clarity, the curves have been vertical shifted. Inset shows the corresponding compensated spectra for both inverse energy cascade and forward enstrophy cascade by using fitting scaling exponents respectively on the range  $3 < k < 20$  and  $100 < k < 1000$ .

238 regimes. The first regime is on the range  $2 \leq k \leq 20$ , corresponding to the inverse energy  
 239 cascade. The another one is on the range  $200 \leq k \leq 2000$ , corresponding to the forward  
 240 enstrophy cascade. Figure 5 b) shows the pdf  $p(C|k)$  on the inverse energy cascade (resp.  
 241  $k = 4, 6, 16$  and  $20$  ). For comparison, the normal distribution is demonstrated by a solid  
 242 line. All the measured pdf has an exponential tail. We note that the pdf in the inverse  
 243 energy cascade does collapse with each other, indicating a nonintermittent cascade. For the  
 244 pdf in the forward enstrophy cascade, they also possess an exponential tail. However, they  
 245 can not collapse with each other due to different shape of the core part  $-5 < C(k)/\sigma < 5$ .  
 246 The exponential tail of the vorticity field consists with very recently theoretical prediction  
 247 by Falkovich and Lebedev<sup>31</sup>.

248 Figure 6 shows the comparison of the measured Hilbert energy spectrum  $\mathcal{L}_2(k)/k$  ( $\square$ ) and  
 249 the Fourier power spectrum  $E_\omega(k)$  (solid line). For display clarity, the curve has been vertical  
 250 shifted. Note that both methods provide the nearly same forward enstrophy cascade on the  
 251 range  $100 < k < 1000$  with a scaling exponent close to  $\simeq 2$ . This scaling exponent agrees

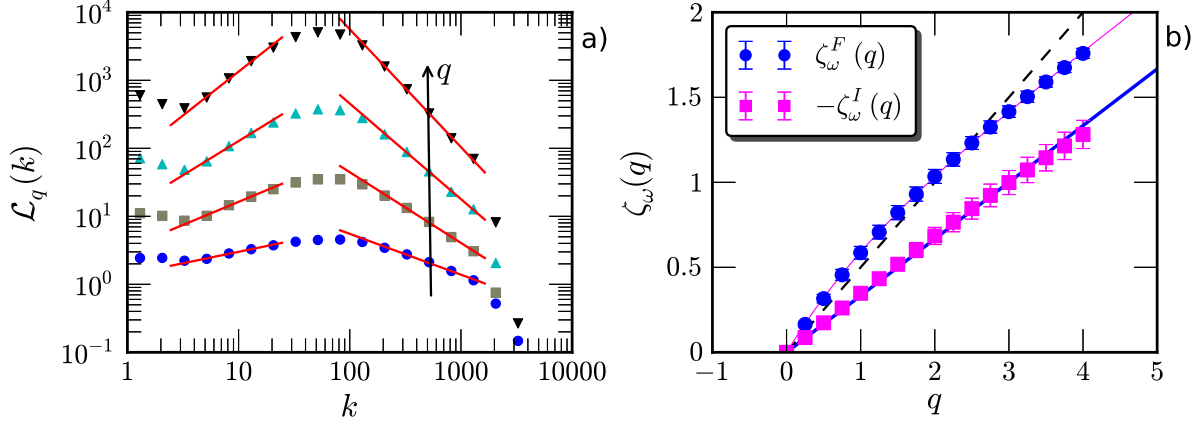


FIG. 7. (Color online) a) Measured  $q$ th-order Hilbert spectra  $\mathcal{L}_q(k)$  for  $q = 1, 2, 3, 4$ . power-law behavior is observed on the range  $200 \leq k \leq 2000$  for the forward enstrophy cascade and on the range  $3 \leq k \leq 20$  for the inverse energy cascade, respectively. The scaling exponents  $\zeta_\omega(q)$  are then estimated on this dual power-law ranges. b) Measured scaling exponents  $\zeta_\omega^F(q)$  ( $\circ$ ) and  $-\zeta_\omega^I(q)$  ( $\square$ ). For comparison, the dashed line is  $q/3$  and the solid line is for a log-Poisson fitting  $\zeta_\omega^F(q) = q/3 + 0.45(1 - 0.43^q)$ . The errorbar indicates 95% fitting confidence.

252 very well with the experimental observation by Kellay, Wu, and Goldburg<sup>26</sup>. We show in  
 253 the inset the compensated curve by using the fitted exponent for the forward cascade (closed  
 254 square for the Hilbert and solid line for Fourier). The observed plateau confirms the power-  
 255 law behavior as expected. Furthermore, we have an additional power-law behavior on the  
 256 range  $3 < k < 20$  for the inverse energy cascade. The compensated spectra are also shown in  
 257 the inset (open square for the Hilbert and dashed line for Fourier) to emphasize the observed  
 258 inverse energy cascade. Both Hilbert and Fourier methodologies identify almost the same  
 259 dual power-law behavior.

260 We now turn to the high-order Hilbert statistics. The convergence of the statistical  
 261 moment  $\mathcal{L}_q(k)$  has been verified by checking the integral kernel  $p(C, k)|C|^q$  at given scales.  
 262 A quite good convergence has been found for all wavenumber  $k$  up to  $q = 4$  (not shown  
 263 here). Figure 7 a) shows the measured  $\mathcal{L}_q(k)$  for  $q = 1, 2, 3$  and 4 (from bottom to top). A  
 264 dual power-law behavior is observed as expected respectively on the range  $3 \leq k \leq 20$  for  
 265 the inverse energy cascade and  $200 \leq k \leq 2000$  for the forward enstrophy cascade. The  
 266 scaling exponent  $\zeta_\omega(q)$  is then estimated respectively on these two ranges by using a least  
 267 square fitting algorithm. Figure 7 b) shows the corresponding measured scaling exponent

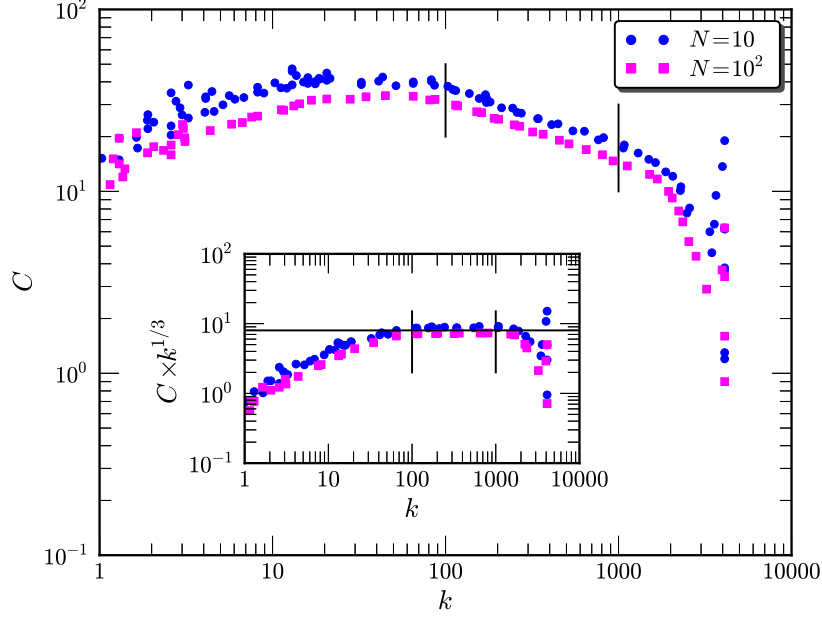


FIG. 8. (Color online) Experimental contour line for  $N = 10$  ( $\circ$ ) and  $N = 100$  ( $\square$ ). power-law behavior is observed on the range  $100 \leq k \leq 1000$  with a scaling exponent  $\simeq 1/3$ . The inset shows the compensated curve by multiplying  $k^{1/3}$ . The observed power-law indicates an asymptotic scaling exponent  $\lim_{q \rightarrow +\infty} \zeta_{\omega}^F(q) = q/3$ .

268  $\zeta_{\omega}(q)$ , in which the errorbar is 95% fitting confidence. For the inverse energy cascade,  
 269 the measured  $\zeta_{\omega}^I(q)$  ( $\square$ ) is linear with  $q$ , i.e.,  $\zeta_{\omega}^I(q) = -q/3$ , confirming that there is no  
 270 intermittent effect in this inverse cascade process.<sup>4</sup> However, the observed  $-q/3$  scaling does  
 271 not consist with the prediction of Eq. (16c). This implies that for the vorticity field some  
 272 important mechanisms are ignored in the previously dimensional arguments of the inverse  
 273 energy cascade. For example, if one takes the enstrophy dissipation  $\eta_{\alpha}$  into account and  
 274 assumes it as important as the Ekman energy dissipation  $\epsilon_{\alpha}$ , one then has the right scaling  
 275 behavior, i.e.,  $\mathcal{L}_q(k) \sim (\epsilon_{\alpha}\eta_{\alpha})^{q/6} k^{q/3}$ . This corresponds to a scaling exponent  $\zeta_{\omega}^I(q) = -q/3$   
 276 for the inverse energy cascade. However, this naive dimensional argument should be justified  
 277 for physical evidence and for more database.

278 The measured scaling exponent  $\zeta_{\omega}^F(q)$  ( $\circ$ ) is also shown in Fig. 7b). We note that when  
 279  $q \leq 2$  the measured  $\zeta_{\omega}^F(q)$  is nonlinear dependent with  $q$ , indicating an intermittent effect of  
 280 the vorticity field. While when  $q \geq 2$ , it seems to be linear with  $q$  with a slope  $\simeq 1/3$ . We  
 281 propose here a log-Poisson-like model for the observed scaling exponent, i.e.,

$$\zeta_{\omega}^F(q) = \gamma q + \mathcal{B}(1 - \varphi^q) \quad (17)$$

282 in which the parameter  $\gamma = 1/3$ ,  $\mathcal{B} = 0.45$  and  $\varphi = 0.43$  are determined as following. For  
 283 large value of  $q$  (if the corresponding statistics exists), the  $q$ th-order Hilbert moments  $\mathcal{L}_q(k)$   
 284 is thus dominated by the tail of the pdf  $p(C, k)$ . Therefore, if the scaling behavior holds,  
 285 the measured joint pdf  $p(C, k)$  should also show a scaling behavior for the contour line.  
 286 We extract the measured contour line for  $p(C, k)$  (in points) with two values  $N = 10$  ( $\circ$ )  
 287 and  $100$  ( $\square$ ), see Fig. 8. Power-law behavior is indeed observed as expected on the range  
 288  $100 \leq k \leq 2000$ . The scaling exponent is found to be  $\simeq 1/3$ . To emphasize the observed  
 289  $1/3$  scaling, the compensated curves  $C(k)k^{1/3}$  are shown as inset of Fig. 8. A clear plateau  
 290 is observed on the expected range  $100 \leq k \leq 2000$ . This yields  $\gamma = 1/3$ . The rest of the  
 291 parameters  $\mathcal{B}$  and  $\varphi$  are then obtained by using a least square fitting algorithm.

## 292 B. Extended Self-Similarity of Structure-Functions

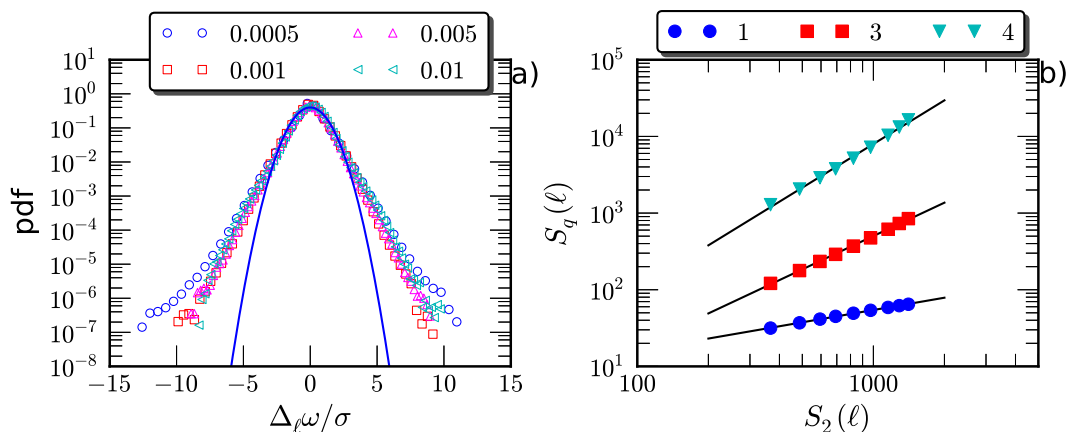


FIG. 9. (Color online) a) Measured pdf for vorticity increments with several separation scales  $\ell$  in the range of the forward enstrophy cascade. The Gaussian distribution is illustrated by a solid line. Note that except for the first scale ( $\ell = 0.0005$ ), they all have an exponential tails and do collapse with each other. b) Extended Self-Similarity plots of the SFs on the range  $0.0005 < \ell < 0.005$ , corresponding to a wavenumber range  $200 < k < 2000$ . The solid line is a power-law fitting on this range by using a least square algorithm. For display clarity, these curves have been vertical shifted.

293 As we shown above that due to the large-scale structure influence the second-order SF  
 294 fails to identify the power-law behavior of the forward enstrophy cascade, see Fig. 3b).  
 295 Here we apply the Extended Self-Similarity (ESS) technique to extract the relative scaling



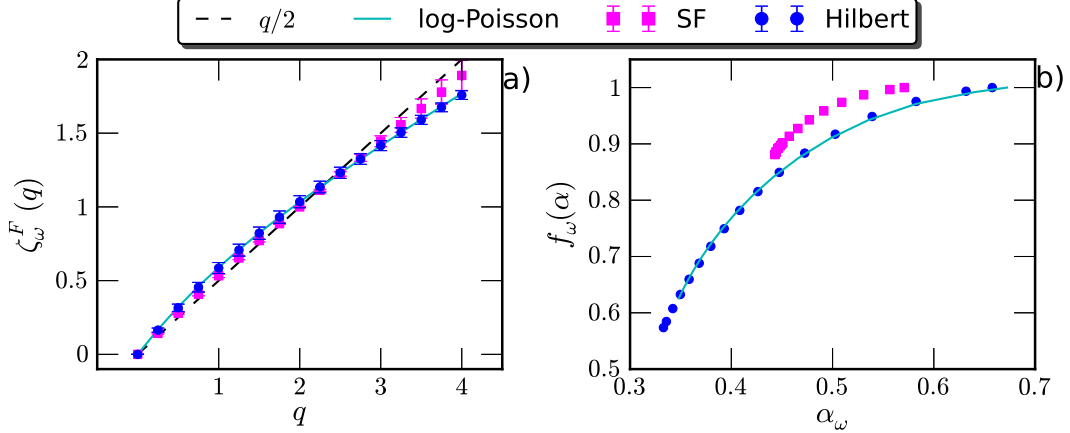


FIG. 10. (Color online) a) Comparison of the measured relative scaling exponents  $\zeta_\omega^E(q)$  for the SFs ( $\square$ ), the scaling exponent  $\zeta_\omega^F(q)$  provided by the Hilbert method ( $\circ$ ) and the log-Poisson fitting (solid line). b) The corresponding singularity spectrum  $f_\omega(\alpha)$ .

296 exponents.<sup>46</sup> Note that for the forward enstrophy cascade, the second-order Hilbert moments  
 297 provides a scaling exponent  $\zeta_\omega^F(2) \simeq 1$  and the Fourier power spectrum provides  $\beta \simeq 2$ .  
 298 Therefore, we define the ESS of the SFs by using the second-order SFs, i.e.,

$$S_q(\ell) \sim (S_q(\ell))^{\zeta_\omega^E(q)} \quad (18)$$

299 in which  $S_q(\ell) = \langle |\Delta_\ell \omega|^q \rangle$ , and  $\zeta_\omega^E(q)$  is the ESS scaling exponent. Figure 9 a) shows the  
 300 measured pdf of the vorticity increment for different separation scales in the forward enstro-  
 301 phy cascade. Except for  $\ell = 0.005$ , all the pdfs have an exponential tail and almost collapse  
 302 with each other. Figure 9 b) shows the ESS plots on the range  $0.0005 < \ell < 0.005$ , corre-  
 303 sponding to a wavenumber range  $200 < k < 2000$ , which is the scaling range of the forward  
 304 enstrophy cascade predicted by the Hilbert method. Power-law behavior is observed for all  $q$   
 305 we considered here. The ESS scaling is estimated on this range by using a least square fitting  
 306 algorithm. Figure 10 a) shows the measured ESS scaling exponent  $\zeta_\omega^E(q)$  ( $\square$ ), in which the  
 307 errorbar indicates the 95% fitting confidence. For comparison, the scaling exponent provided  
 308 by the Hilbert method ( $\circ$ ) is also shown. Graphically, the measured  $\zeta_\omega^E(q)$  indicates a less  
 309 intermittent vorticity field. To emphasize this point, the singularity spectrum  $f_\omega(\alpha)$  is then  
 310 calculated, i.e.,

$$\alpha_\omega = \zeta_\omega(q)', \quad f_\omega(\alpha) = \min \{ \alpha_\omega q - \zeta_\omega(q) + 1 \} \quad (19)$$

311 in which the scaling exponents  $\zeta_\omega(q)$  could be either scaling exponent from Hilbert method  
 312 or one from the SFs. Figure 10 b) shows the measured  $f_\omega(\alpha)$  for the forward enstrophy

313 cascade, in which the log-Poisson fitting is illustrated by a solid line. It confirms again that  
314 the SFs predicts a less intermittent vorticity field.

### 315 C. Discussion

316 Several works have been reported for the forward enstrophy cascade that the Fourier  
317 power spectrum of vorticity field possesses a ‘ $-2$ ’ power-law behavior rather than ‘ $-1$ ’ one  
318 required by Kraichnan’s theory, see Eq. (3). However, there is no theory explanation for this  
319 contradiction. Specifically for the Hilbert method, we note that the second-order statistics  
320  $\mathcal{L}_2(k)$  provides  $\zeta_\omega^F(2) \simeq 1.0$  (resp. ‘ $-2.0$ ’ for the Hilbert energy spectrum) rather than 0  
321 required by the dimensional argument. The high-order scaling exponents  $\zeta_\omega(q)$  provided  
322 by the Hilbert method for both the inverse energy cascade and forward enstrophy cascade  
323 disagree with the Kraichnan’s theory prediction, see Eq. (16).<sup>7,22</sup> Furthermore, they do not  
324 agree with the logarithmic correction theory either.<sup>7</sup> It suggests that a new theory is required  
325 in future to interpret the vorticity field of 2D turbulence to take into account not only this  
326 inconsistency but also the intermittent effect.

327 We emphasize here that the scaling property of the forward enstrophy cascade might  
328 depend on the Ekman friction, the parameter  $\alpha$ .<sup>20,21,25</sup> Therefore, more data sets should be  
329 certainly investigated in future to see whether the scaling behavior reported in this work is  
330 universal for different  $\alpha$ .

## 331 V. CONCLUSION

332 In summary, we have applied the Hilbert methodology to the vorticity field obtained from  
333 a high resolution DNS of 2D turbulence. A dual-cascade with almost one decade scales for the  
334 inverse energy cascade and forward enstrophy cascade is identified. The scaling exponents  
335  $\zeta_\omega(q)$  are extracted. In the inverse energy cascade, the pdf  $p(C, k)$  is collapsed with each  
336 other with an exponential tail. This indicates a nonintermittent cascade process, which  
337 is confirmed by the measured scaling exponent  $\zeta_\omega^I(q) = -q/3$ . In the forward enstrophy  
338 cascade, the measured pdf  $p(C, k)$  also have an exponential tail. However, due to the different  
339 shape of the core part, they can not collapse with each other, indicating an intermittent  
340 forward enstrophy cascade. The measured scaling exponent  $\zeta_\omega^F(q)$  is nonlinear with  $q$  when

341  $q \leq 2$ , showing intermittency. A log-Poisson fitting, i.e.,  $\zeta_\omega^F(q) = q/3 + 0.45(1 - 0.43^q)$ , is  
342 thus proposed to characterize the measured  $\zeta_\omega^F(q)$ .

### 343 ACKNOWLEDGMENTS

344 This work is sponsored by the National Natural Science Foundation of China under  
345 Grant (Nos. 11072139, 11032007, 11272196, 11202122 and 11332006) , ‘Pu Jiang’ project  
346 of Shanghai (No. 12PJ1403500) and the Shanghai Program for Innovative Research Team  
347 in Universities. We thank Professor G. Boffetta for providing us the DNS data, which  
348 is freely available from the iCFDdatabase.<sup>47</sup> Y.H. thanks Prof. L. Biferale and Prof. G.  
349 Falkovich for useful discussions and comments. We thank Dr Gabriel Rilling and Professor  
350 Patrick Flandrin from laboratoire de Physique, CNRS & ENS Lyon (France) for sharing  
351 their EMD code with us.<sup>48</sup> We also thank the anonymous referees for their useful comments  
352 and suggestions.

### 353 REFERENCES

- 354 <sup>1</sup>R. Kraichnan and D. Montgomery, “Two-dimensional turbulence,” *Rep.Prog. Phys.* **43**,  
355 547 (1980).
- 356 <sup>2</sup>P. Tabeling, “Two-dimensional turbulence: a physicist approach,” *Phys. Rep.* **362**, 1–62  
357 (2002).
- 358 <sup>3</sup>H. Kellay and W. Goldberg, “Two-dimensional turbulence: a review of some recent ex-  
359 periments,” *Rep. Prog. Phys.* **65**, 845 (2002).
- 360 <sup>4</sup>G. Boffetta and R. Ecke, “Two-dimensional turbulence,” *Annu. Rev. Fluid Mech.* **44**,  
361 427–51 (2012).
- 362 <sup>5</sup>F. Bouchet and A. Venaille, “Statistical mechanics of two-dimensional and geophysical  
363 flows,” *Phys. Rep.* **515**, 227–95 (2012).
- 364 <sup>6</sup>R. Irion, “Soap films reveal whirling worlds of turbulence,” *Science* **284**, 1609–1610 (1999).
- 365 <sup>7</sup>G. Falkovich and V. Lebedev, “Universal direct cascade in two-dimensional turbulence,”  
366 *Phys. Rev. E* **50**, 3883 (1994).
- 367 <sup>8</sup>S. Chen, R. Ecke, G. Eyink, X. Wang, and Z. Xiao, “Physical mechanism of the two-  
368 dimensional enstrophy cascade,” *Phys. Rev. Lett.* **91**, 214501 (2003).

- 369 <sup>9</sup>S. Chen, R. Ecke, G. Eyink, M. Rivera, M. Wan, and Z. Xiao, “Physical mechanism of  
370 the two-dimensional inverse energy cascade,” *Phys. Rev. Lett.* **96**, 84502 (2006).
- 371 <sup>10</sup>G. Boffetta and S. Musacchio, “Evidence for the double cascade scenario in two-  
372 dimensional turbulence,” *Phys. Rev. E* **82**, 016307 (2010).
- 373 <sup>11</sup>A. Alexakis and C. Doering, “Energy and enstrophy dissipation in steady state 2D turbu-  
374 lence,” *Phys. Lett. A* **359**, 652–657 (2006).
- 375 <sup>12</sup>H. Xia, D. Byrne, G. Falkovich, and M. Shats, “Upscale energy transfer in thick turbulent  
376 fluid layers,” *Nature Phys.* **7**, 321–324 (2011).
- 377 <sup>13</sup>H. Xia, H. Punzmann, G. Falkovich, and M. Shats, “Turbulence-condensate interaction  
378 in two dimensions,” *Phys. Rev. Lett.* **101**, 194504 (2008).
- 379 <sup>14</sup>T. Tran, P. Chakraborty, N. Guttenberg, A. Prescott, H. Kellay, W. Goldburg, N. Gold-  
380 enfeld, and G. Gioia, “Macroscopic effects of the spectral structure in turbulent flows,”  
381 *Nature Phys.* **6**, 438–441 (2010).
- 382 <sup>15</sup>D. Kelley and N. Ouellette, “Spatiotemporal persistence of spectral fluxes in two-  
383 dimensional weak turbulence,” *Phys. Fluids* **23**, 115101–115101 (2011).
- 384 <sup>16</sup>S. Merrifield, D. Kelley, and N. Ouellette, “Scale-dependent statistical geometry in two-  
385 dimensional flow,” *Phys. Rev. Lett.* **104**, 254501 (2010).
- 386 <sup>17</sup>A. Celani, S. Musacchio, and D. Vincenzi, “Turbulence in more than two and less than  
387 three dimensions,” *Phys. Rev. Lett.* **104**, 184506 (2010).
- 388 <sup>18</sup>N. Khurana and N. Ouellette, “Interactions between active particles and dynamical struc-  
389 tures in chaotic flow,” *Phys. Fluids* **24**, 091902–091902 (2012).
- 390 <sup>19</sup>G. Van Heijst and H. Clercx, “Laboratory modeling of geophysical vortices,” *Annu. Rev.*  
391 *Fluid Mech.* **41**, 143–164 (2009).
- 392 <sup>20</sup>G. Boffetta, A. Celani, S. Musacchio, and M. Vergassola, “Intermittency in two-  
393 dimensional Ekman-Navier-Stokes turbulence,” *Phys. Rev. E* **66**, 026304 (2002).
- 394 <sup>21</sup>G. Boffetta, “Energy and enstrophy fluxes in the double cascade of two-dimensional tur-  
395 bulence,” *J. Fluid Mech.* **589**, 253–260 (2007).
- 396 <sup>22</sup>R. Kraichnan, “Inertial ranges in two-dimensional turbulence,” *Phys. Fluids* **10**, 1417–1423  
397 (1967).
- 398 <sup>23</sup>U. Frisch, *Turbulence: the legacy of AN Kolmogorov* (Cambridge University Press, 1995).
- 399 <sup>24</sup>Y. Huang, F. Schmitt, Z. Lu, P. Fougairolles, Y. Gagne, and Y. Liu, “Second-order  
400 structure function in fully developed turbulence,” *Phys. Rev. E* **82**, 026319 (2010).

- 401 <sup>25</sup>L. Biferale, M. Cencini, A. Lanotte, and D. Vergni, “Inverse velocity statistics in two-  
402 dimensional turbulence,” *Phys. Fluids* **15**, 1012–1020 (2003).
- 403 <sup>26</sup>H. Kellay, X. Wu, and W. Goldburg, “Vorticity measurements in turbulent soap films,”  
404 *Phys. Rev. Lett.* **80**, 277–280 (1998).
- 405 <sup>27</sup>J. Paret, M. Jullien, and P. Tabeling, “Vorticity statistics in the two-dimensional enstrophy  
406 cascade,” *Phys. Rev. Lett.* **83**, 3418–3421 (1999).
- 407 <sup>28</sup>K. Nam, E. Ott, T. Antonsen Jr, and P. Guzdar, “Lagrangian chaos and the effect of drag  
408 on the enstrophy cascade in two-dimensional turbulence,” *Phys. Rev. Lett.* **84**, 5134–5137  
409 (2000).
- 410 <sup>29</sup>D. Bernard, “Influence of friction on the direct cascade of the 2D forced turbulence,”  
411 *Europhys. Lett.* **50**, 333 (2000).
- 412 <sup>30</sup>Y. Tsang, E. Ott, T. Antonsen Jr, and P. Guzdar, “Intermittency in two-dimensional  
413 turbulence with drag,” *Phys. Rev. E* **71**, 066313 (2005).
- 414 <sup>31</sup>G. Falkovich and V. Lebedev, “Vorticity statistics in the direct cascade of two-dimensional  
415 turbulence,” *Phys. Rev. E* **83**, 045301 (2011).
- 416 <sup>32</sup>G. Falkovich and K. R. Sreenivasan, “Lessons from hydrodynamic turbulence,” *Phys.*  
417 *Today* **59**, 43 (2006).
- 418 <sup>33</sup>Y. Huang, F. Schmitt, Z. Lu, and Y. Liu, “An amplitude-frequency study of turbulent  
419 scaling intermittency using Hilbert spectral analysis,” *Europhys. Lett.* **84**, 40010 (2008).
- 420 <sup>34</sup>Y. Huang, F. Schmitt, J.-P. Hermand, Y. Gagne, Z. Lu, and Y. Liu, “Arbitrary-order  
421 Hilbert spectral analysis for time series possessing scaling statistics: comparison study  
422 with detrended fluctuation analysis and wavelet leaders,” *Phys. Rev. E* **84**, 016208 (2011).
- 423 <sup>35</sup>N. E. Huang, Z. Shen, S. R. Long, M. C. Wu, H. H. Shih, Q. Zheng, N. Yen, C. C.  
424 Tung, and H. H. Liu, “The empirical mode decomposition and the Hilbert spectrum for  
425 nonlinear and non-stationary time series analysis,” *Proc. R. Soc. London, Ser. A* **454**,  
426 903–995 (1998).
- 427 <sup>36</sup>N. E. Huang, Z. Shen, and S. R. Long, “A new view of nonlinear water waves: The Hilbert  
428 Spectrum ,” *Annu. Rev. Fluid Mech.* **31**, 417–457 (1999).
- 429 <sup>37</sup>P. Flandrin and P. Gonçalves, “Empirical mode decompositions as data-driven Wavelet-  
430 like expansions,” *Int. J. Wavelets, Multires. Info. Proc.* **2**, 477–496 (2004).
- 431 <sup>38</sup>G. Rilling, P. Flandrin, and P. Gonçalves, “On empirical mode decomposition and its al-  
432 gorithms,” *IEEE-EURASIP Workshop on Nonlinear Signal and Image Processing* (2003).

- 433 <sup>39</sup>Y. Huang, *Arbitrary-Order Hilbert Spectral Analysis: Definition and Application to fully*  
434 *developed turbulence and environmental time series*, Ph.D. thesis, Université des Sciences  
435 et Technologies de Lille - Lille 1, France & Shanghai University, China (2009).
- 436 <sup>40</sup>L. Cohen, *Time-frequency analysis* (Prentice Hall PTR Englewood Cliffs, NJ, 1995).
- 437 <sup>41</sup>P. Flandrin, *Time-frequency/time-scale analysis* (Academic Press, 1998).
- 438 <sup>42</sup>Y. Huang, L. Biferale, E. Calzavarini, C. Sun, and F. Toschi, “Lagrangian single particle  
439 turbulent statistics through the Hilbert-Huang transforms,” *Phys. Rev. E* **87**, 041003(R)  
440 (2013).
- 441 <sup>43</sup>C. Pasquero and G. Falkovich, “Stationary spectrum of vorticity cascade in two-  
442 dimensional turbulence,” *Phys. Rev. E* **65**, 56305 (2002).
- 443 <sup>44</sup>P. A. Davidson and B. R. Pearson, “Identifying turbulent energy distribution in real, rather  
444 than fourier, space,” *Phys. Rev. Lett.* **95**, 214501 (2005).
- 445 <sup>45</sup>F. Toschi, L. Biferale, G. Boffetta, A. Celani, B. Devenish, and A. Lanotte, “Acceleration  
446 and vortex filaments in turbulence,” *J. Turbu.* **6**, 15 (2005).
- 447 <sup>46</sup>R. Benzi, S. Ciliberto, R. Tripiccione, C. Baudet, F. Massaioli, and S. Succi, “Extended  
448 self-similarity in turbulent flows,” *Phys. Rev. E* **48**, 29–32 (1993).
- 449 <sup>47</sup><http://cfd.cineca.it>.
- 450 <sup>48</sup><http://perso.ens-lyon.fr/patrick.flandrin/emd.html>.